p 145.
(46) F. Hajdu, *Acta Crystallogr., Sect. A*, **27**, 73 (1971); G. Palinkas, *ibid.*, **29**, 10 (1973).
(47) F. Hajdu, *Acta Crystallogr., Sect. A*, **28**, 250 (1972), and private communications.
(48) R. M. Lawrence and R. F. Kruh, *J. Chem. Phys.*, **41**, 4758 (1967).
(49) J. H. Konnert and J. Karle, *Acta Crystallogr., Sect. A*, **29**, 702 (1973).
(50) J. Waser and V. Schomaker, *Rev. Mod. Phys.*, **25**, 671 (1953).
(51) D. L. Wertz and J. R. Bell, *J. Inorg. Nucl. Chem.*, **35**, 137, 861 (1973).
(52) D. H. Templeton and C. H. Dauben, *J. Am. Chem. Soc.*, **75**, 6069 (1953).
(53) P. Polx, *C. R. Acad. Sci., Ser. C*, **270**, 1852 (1970).
(54) $n_1 = 7.6 \times 10^3\ e^2/9.5 \times 10^2\ e^2 = 8.0$.
(55) Assuming $n_1 + n_2 = 8$, then $n_1 \simeq 6.0$ and $n_2 \simeq 2.0$ to satisfy the relationship $1.05 \times 10^4\ e^2 = n_1 \times 9.5 \times 10^2\ e^2 + n_2 \times 2.4 \times 10^3\ e^2$.
(56) S. C. Lee and R. Kaplow, *Science*, **169**, 477 (1970).
(57) D. L. Wertz, *J. Solution Chem.*, **1**, 489 (1972).
(58) R. M. Lawrence and R. F. Kruh, *J. Chem. Phys.*, **47**, 4758 (1967).
(59) D. L. Wertz and R. F. Kruh, *J. Chem. Phys.*, **50**, 4313 (1969).
(60) J. N. Albright, *J. Chem. Phys.*, **56**, 3783 (1972).
(61) J. R. Bell and D. L. Wertz, *J. Am. Chem. Soc.*, **95**, 1456 (1973).
(62) J. L. Tyvoll and D. L. Wertz, *J. Inorg. Nucl. Chem.*, **36**, 3713 (1974).

Quadrupole Coupling Constants of Square-Planar Copper(II)–Sulfur Complexes from Single-Crystal Electron Paramagnetic Resonance Spectroscopy

Lawrence K. White and R. Linn Belford*

Contribution from the Department of Chemistry, University of Illinois, Urbana, Illinois 61801. *Received September 2, 1975*

Abstract: The nuclear quadrupole coupling parameters are measured for copper in six square-planar complexes, five having sulfur donor atoms and one having both sulfur and oxygen donors. Computer simulations of the EPR spectra of the Cu-doped powders are employed to refine the principal g and A values. The secondary ($\Delta m_I = 1$) transitions of the EPR spectra of Cu-doped single crystals are analyzed for the quadrupole coupling parameters. The small quadrupole coupling constant for the $Cu-S_4$ complexes ($QD \approx 0.7 \times 10^{-4}\ cm^{-1}$) implies an effectively spherical symmetry which is attributed chiefly to the large covalent character of the Cu–S σ bond. A few anomalies are observed in the quadrupole data. A larger quadrupole coupling constant is observed for diethyl dithiophosphate, $Cu(S_2P(OC_2H_5)_2)_2$, than for other $Cu-S_4$ complexes studied, i.e., 1.8×10^{-4} cm^{-1} compared to $0.7 \times 10^{-4}\ cm^{-1}$. Also, a large asymmetry parameter (QE) is observed for the bis(maleonitriledithiolate) copperate(II), $Cu(mnt)_2^{2-}$, dianion and the mixed S–O square-planar complex copper(II) bis(*cis*-monothiodibenzoylmethanate), $Cu(SdbmO)_2$. The quadrupole coupling parameters may be sensitive to Cu–P transannular interaction in $Cu(S_2P(OC_2H_5)_2)$ and to the strong complex π bonding present in $Cu(mnt)_2^{2-}$.

I. Introduction

In the early 1950's Bleaney[1-3] suggested that quadrupole coupling data could be obtained from single-crystal EPR studies. So and Belford[4,5] examined the secondary (or forbidden $\Delta m_I = \pm 1$) transitions in the single-crystal EPR spectra of several Cu–O complexes, including four square-planar β-ketoenolates (typified by $Cu(acac)_2$, bis(2,4-pentanedionato)copper(II), I) and one square-planar copper(II)–sulfur complex ($Cu(dtc)_2$, bis(diethyldithiocarbamate)-copper(II), II). Recently we reported[6] the quadrupole coupling

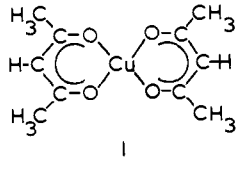

I

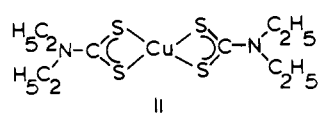

II

constant of another square-planar Cu–O complex ($Cu(C_2O_4)_2^{2-}$, bis(oxalato)cuprate(II) dianion, III). These studies have been continued. Here we study several copper(II)–sulfur complexes of square-planar geometry to determine the sensitivity of the quadrupole coupling parameter to more subtle aspects of the electronic structures of the molecules. The quadrupole coupling parameters are obtained from the single-crystal EPR spectra for five square-planar Cu–S complexes: $Cu(dto)_2^{2-}$, bis(dithiooxalate) cuprate(II), IV; $Cu(i\text{-}mnt)^{-2}$, bis(1,1-dicyano-2,2-dithioethylene)cuprate(II), V; $Cu(dtc)_2^{2-}$, II, EPR data repeated; $Cu(S_2P(OC_2H_5)_2)_2$, bis-(diethyl dithiophosphate)coppe!(II) (in Ni host), VI; and $Cu(mnt)_2^{2-}$, bis(1,2-dicyano-1,2-dithioethylene)cuprate(II), VII. We also report data for one mixed sulfur–oxygen donor

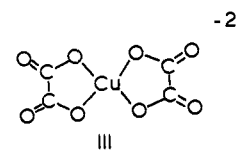

III

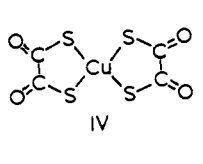

IV

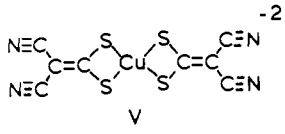

V

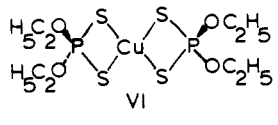

VI

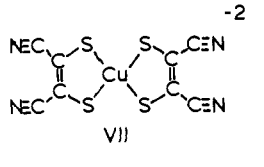

VII

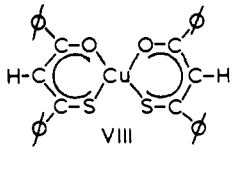

VIII

complex $Cu(SdbmO)_2$, copper(II) bis(*cis*-monothiodibenzoylmethanate) (VIII).

We have employed EPR data obtained from computer simulation of powdered samples to help analyze the single-crystal EPR spectra for these nearly axial systems. The features of the EPR spectrum of a powder are extremely sensitive to the magnitude of the principal g and A values; easily obtainable precisions are ± 0.0003 for g and $\pm 0.3 \times 10^{-4}\ cm^{-1}$ for A. Since the hyperfine interaction in these compounds is much larger than either the nuclear Zeeman or nuclear quadrupole interaction, neither the line positions nor intensities of the primary ("allowed" $\Delta M_I = 0$) transitions are affected substantially by these interactions. Only the electronic Zeeman

and hyperfine interactions need to be included in computer simulations of the primary transitions in the EPR spectrum of powders. Refined principal g and A values obtained from the powder EPR spectra were used to analyze the secondary ($\Delta m_I = \pm 1$, forbidden) doublet spacings for the quadrupole coupling parameters.

II. Quadrupole Coupling and Electron Paramagnetic Resonance

The general theory and origin of the quadrupole interaction have been discussed by several authors.[7-9] In brief, the quadrupolar coupling arises from the electrostatic interaction between a quadrupolar nucleus, one with $I \geq 1$, and its surrounding charges. It reflects the anisotropy in the charge distribution of the system. The quadrupole coupling contant, $eqeQ$, is the product of the quadrupole moment of the nucleus, eQ, and the major electric field gradient, eq, at the nucleus. The moment, eQ, is a measure of the anisotropic distribution of charge within the nucleus. The gradient, eq, is a measure of the anisotropic distribution of charge surrounding that nucleus. The discussion below is for nuclei of spin $\frac{3}{2}$.

The quadrupole interaction energy can be represented by $\mathbf{I}\cdot\mathbf{Q}\cdot\mathbf{I}$, containing the quadrupole tensor, $\mathbf{Q}$. For the coordinate frame, in which the nuclear quadrupole tensor is diagonal, the quadrupolar part of the spin Hamiltonian is $\mathcal{H}_q = Q_x I_x^2 + Q_y I_y^2 + Q_z I_z^2$, where $Q_p = eQeq_p/4$, $p = x, y, z$. However, since the quadrupole tensor is traceless, $Q_x + Q_y + Q_z = 0$, the spin Hamiltonian can be represented as follows:

$$\mathcal{H}_q = QD[I_z^2 - I(I+1)/3] + QE(I_x^2 - I_y^2)$$

where $QD = Q_z - \frac{1}{2}(Q_x + Q_y)$ and $QE = \frac{1}{2}(Q_x - Q_y)$. Note that the presence of operators of only nuclear spin means that just the energy levels of the nucleus are directly affected by the quadrupole interaction. If QE equals zero, the system is axial or has cylindrical charge distribution. Deviation from an axial charge distribution is denoted by a nonzero QE. Most of the systems considered here are essentially axial; thus QD is sufficient to give complete information on the magnitude and sign of the quadupolar coupling.

The chemical information desired from quadrupole coupling data is the electric field gradient (EFG). Since the EFG is the second derivative of the electric potential, $\partial^2 V/\partial^2 p$, it is a direct measure of the electronic charge distribution around the quadrupolar nucleus. The EFG can be obtained only if the quadrupole moment (eQ) is known.

Although there are several ways of measuring quadrupole coupling constants, most have severe experimental limitations. The major limitation and advantage of EPR is its exclusive use for paramagnetic systems. Nuclear quadrupole resonance (NQR), the traditional method for measuring the quadrupole coupling constants, seldom can be used for paramagnetic systems, owing to their rapid relaxation times. The EPR technique is also far more sensitive than radiofrequency methods. All that is necessary to obtain quadrupole coupling information is a host crystal the size of a pinhead doped with no more than micrograms of paramagnetic material. The usual NQR experiment requires grams of sample.

Natural-abundance copper contains two quadrupolar nuclei, ^{63}Cu and ^{65}Cu. Each has $I = \frac{3}{2}$. Since the nuclear g value of ^{65}Cu, 1.5871, is slightly larger than that of ^{63}Cu, 1.4812,[10] the EPR spectrum is complicated by doubled and often partly overlapping hyperfine structure. In most cases the best data can be obtained from a ^{63}Cu-doped host lattice, although occasionally sufficiently good data can be obtained from host lattices doped with natural-abundance copper.

The quadrupole moment, $Q = -0.211$ b,[11] is known for the ^{63}Cu nucleus and its magnitude is large enough to give quadrupole coupling constants that can be measured well through precise single-crystal EPR studies.

III. Experimental Section

A. EPR Spectra. Because of a smaller nuclear Zeeman term, the secondary transitions have very weak intensities in the X band, 9.5-GHz, spectra; thus, quadrupole coupling data could only be obtained from Q-band, 35-GHz, EPR single-crystal spectra.

Q-Band, 35.0-GHz, EPR spectra were taken on a Varian E-15 spectrometer, with a DPPH (diphenylpicrylhydrazyl) g marker. Since the same magnet was used for wide-line NMR experiments, the magnetic field was calibrated with hydrogen nuclei; otherwise, the magnetic field displayed on the Varian field control was generally assumed to be correct. The frequency had to be calculated from the g marker because the passive frequency meter in the Q-band microwave bridge is not sufficiently accurate. The range of the operating microwave frequencies was 34.5–35.5 GHz. All samples were at room temperature.

The following general procedure was used for all the single-crystal EPR studies. A powder EPR spectrum of the doped crystal was taken. The $g_\parallel$ and $g_\perp$ values were confirmed and refined by computer simulations of the powder EPR spectrum (see Results). The doped single crystals were then mounted in an arbitrary plane. The perpendicular orientation, corresponding to $g_\perp$ and $A_\perp$, was found for this plane and single-crystal EPR spectra were taken at appropriate angular intervals as the crystal was rotated. The most nearly parallel orientation, 90° away from the perpendicular, was recorded. The minimum θ orientation at the most parallel position was calculated by the formula: $g^2 = g_\parallel^2 \cos^2\theta + g_\perp^2 \sin^2\theta$. The real θ orientation for every single-crystal spectrum in the arbitrary plane can be calculated by use of the formulas derived in Appendix A of White's thesis.[42]

Since most of the complexes studied have nearly axial g tensors, the calculated θ orientation is reasonably accurate to ±1.0°. In most cases, the secondary ($\Delta m_I = \pm 1$) transitions that are observed at orientations a few degrees away from the $g_\perp$ position can be followed easily and assigned the appropriate θ orientation.

Some of the complexes examined had quadrupole tensors that were not axial. For them, it was necessary to know the φ orientation, i.e., orientation in the x–y molecular plane. Precession or Weissenberg x-ray photographs were taken in these cases to determine the relationship between morphology and cell orientation of the crystal. The molecular orientation within the crystal was determined from the single-crystal x-ray structure. Crystals were mounted in appropriate orientations with the aid of paraffin wedges.

The computer program used for simulating the EPR spectrum of powder is similar to that of Pilbrow and co-workers;[12-14] second-order perturbation formulas for an orthorhombic spin Hamiltonian generate the line positions of the primary transitions.[12-15] Line intensities are weighted for the anisotropic g; i.e., intensities are proportional to $[g_x^2 g_y^2 \sin^2\theta + g_y^2 g_z^2 (\sin^2\varphi + \cos^2\theta\cos^2\varphi) + g_z^2 g_x^2 (\cos^2\varphi + \cos^2\theta\sin^2\varphi)]/g^2$.[16] The major modification is that a more efficient method is used to integrate over all the possible orientations of θ and φ. Instead of selecting a fine grid of θ and φ orientations that can be simply added to give a smooth powder spectrum, a three-point, Gauss-point integration is used. The powder EPR spectrum ($f(B)$) is a summation of the hyperfine peaks integrated over all θ and φ orientations as shown below:

$$f(B) = \sum_{m=1}^{n} \int_{\theta=0°}^{90°} \int_{\varphi=0°}^{90°} P(m,\theta,\varphi) G(B,m,\theta,\varphi) \sin\theta \, d\theta d\varphi$$

With the integrals approximated by sums, we have

$$f(B) = \sum_m \sum_k \sum_l T_{kl} P(m,\theta_k,\varphi_l) G(B,m,\theta_k,\varphi_l) \sin\theta_k$$

where $P(m,\theta,\varphi)$ is the intensity weighting function. $C(B,m,\theta,\varphi)$, the line width function, includes the line center positions, $B_0(m,\theta,\varphi)$. For the cases reported here, we used Lorentzian line shapes independent of orientation and line number: $G(B,m,\theta,\varphi) = 1/w\pi(1 + [B - B_0(m,\theta,\varphi)]^2/w^2)$, w being the half-width at half-height. T_{kl} is the appropriate weighting factor for the finite difference integration formula. Using a Gauss-point form, one integrates by using higher order polynomials to fit the integration curve. The θ and φ orientations from which G and P are calculated have to be chosen carefully and provided with a proper weighting factor, T_{kl}. The method of point selection and weighting factors for a three-point Gauss-point method

is described in many references; see, for example, Krylov.[17] The powder EPR spectrum, $f(B)$, synthesized by a Gauss-point method, differs from that generated by a uniform grid method only in the selection of θ and φ orientations and an additional weighting factor in T_{kl}.

Calculations employed an IBM 360 computer and the simulated spectrum was displayed on a CALCOMP plotter.

Although the magnitudes of the g and A EPR parameters can be obtained reliably from the powder spectrum, the direction of the g and A tensors with respect to molecule's geometry can only be obtained from single-crystal EPR studies. When no previous single-crystal EPR studies were available, the g_z and A_z directions are assumed to correspond to the obvious molecular z axis.

B. Synthesis and Doping of Host Lattices. Potassium Nickel(II) Bis(dithiooxalate), $K_2Ni(dto)_2$. The nickel and copper dithiooxalate complexes were made according to literature procedures.[18,19] The potassium dithiooxalate ligand was obtained from Eastman Kodak. Crystals, dark purple iridescent prisms, of the nickel complex were obtained by recrystallization from hot water. To yield the best crystals, the nickel complex was synthesized by adding the nickel solution to the ligand solution. To dope the nickel host properly (1 mol %) required approximately a 1:10 Cu/Ni molar ratio. Owing to the large amount of copper complex necessary, we synthesized only natural-abundant copper-doped crystals. The single-crystal EPR spectra showed only one magnetic site, consistent with the nickel crystal's $A2/a$ space group.[19]

Nickel(II) Bis(Diethyldithiocarbamate), $Ni(dtc)_2$. $Ni(dtc)_2$ crystals were grown from $^{63}CuCl_2$ added to a solution of the host $Ni(dtc)_2$ in $CCl_4 + CHCl_3$. Slow evaporation produced large dark-red cubes. The crystal structure of the nickel host has been reported and the single-crystal EPR spectra showed two magnetic sites consistent with its $P2_1/c$ space group.[20]

Bis(1,1-dicyanoethylene-2,2-dithiolate)nickelate(II) Dianion, $Ni(i\text{-}mnt)_2^{2-}$. The sodium salt of the ligand[21] and the Ni and Cu complexes, using tetramethylammonium as the cation, were made according to literature procedures.[22] Crystals of the nickel complex were grown by slow evaporation of an ethanol–acetone solution, 40:60 v/v. Although pure $Cu(i\text{-}mnt)_2^{2-}$ complex was never isolated, crystals of the nickel complex were doped with natural-abundance Cu by adding the Cu synthesis product (10 mol %) to the nickel complex. But only 0.1 mole % actually becomes doped into the nickel complex. The single-crystal EPR spectra showed only one magnetic site.

Nickel Bis(diethyldithiophosphate), $Ni(S_2P(OC_2H_5)_2)_2$. To grow ^{63}Cu-doped single-crystals of $Ni(S_2P(OC_2H_5)_2)_2$, $^{63}CuCl_2$ was added (1 mol %) to a solution of the $Ni(S_2P(OC_2H_5)_2)_2$ in ethanol–acetone. Slow evaporation produced large purple plates. Two magnetic sites were observed in the single-crystal EPR spectra. This observation is consistent with the nickel crystal's x-ray structure and $P2_1/c$ space group.[23,24]

Bis(maleonitriledithiolate)nickelate(II) Dianion, $Ni(mnt)_2^{2-}$. The sodium salt of maleonitriledithiolate, 1,2-dicyanoethylene-1,2-dithiolate, was made according to Bahr.[25] With tetramethylammonium as a cation, both the Ni and ^{63}Cu complexes were made.[26] Crystals were grown of the Ni and ^{63}Cu complexes in a 50:1 molar ratio. Slow evaporation of the chloroform–ethanol solutions produced large red crystals. The crystal structure of the nickel host has been reported and the single-crystal EPR spectra showed only one magnetic site consistent with the $C\bar{1}$ space group.[27,28]

Palladium(II) Bis(*cis*-monothiodibenzoylmethanate), $Pd(SdbmO)_2$. The ligand, monothiodibenzoylmethane, was made and its Ni, Pd, and Cu complexes were prepared according to literature procedures.[29,30] Since no suitable crystals were obtained from the nickel complex, the palladium complex was used as the host. Because of the large amounts of copper required for the $Cu(SdbmO)_2$ synthesis, only natural-abundant Cu was used for doping. The copper complex was made by reaction of the ligand with a $CuCO_3$ suspension in acetone. The Pd–complex synthesis using K_2PdCl_4 gave better results when 1:2 metal/ligand molar ratios were used. If the ligand was in excess, it tended to form an oil when the water solution was added to the acetone solution. Crystals were grown from chloroform–ethanol solutions, 60:40 by volume. They were doped with 1:50 molar ratios of Cu/Pd.

Preliminary EPR studies of the Cu-doped Pd complex showed two magnetic sites and the presence of a second compound in about 5%, with slightly higher g values than the main species. Thin layer chromatography in chloroform on both the Pd and Cu complexes showed two compounds in each. Chromatography on silica gel using chloroform as eluent isolated the major component in the eluent and left the minor component on the column. Eluting with ethyl acetate takes the minor component off the column. Repeated syntheses gave varying amounts of the minor component. Doped crystals grown from the major Cu and Pd components showed a single-crystal EPR spectrum with most of the impurity gone. The identity of the minor component is unknown. We presume the major component to be the cis isomer of the square-planar complex; this assumption is based on the x-ray structure data collected by Shugam[31] for $Pd(SdbmO)_2$.

IV. Analysis of Single-Crystal EPR Spectra

There are many possible strategies for obtaining quadrupole coupling constants from single-crystal EPR data; we have focused upon three features: (1) line positions of the "forbidden" lines (the $\Delta m_I = \pm 1$, *secondary lines*, or sometimes the $\Delta m_I = \pm 2$, *tertiary lines*); (2) intensity of the secondary lines; and (3) line positions of the "allowed" lines ($\Delta m_I = 0$, *primary lines*).

The most sensitive and reliable method, analysis of the line positions of the secondary transitions, is particularly useful for the square-planar copper–sulfur complexes, since their quadrupole coupling constants are small and hardly affect the features of the primary spectrum. An attempt to analyze the line positions of the primary lines at the perpendicular orientation for these complexes was unsuccessful. The spacings between the primary transitions must be accurate to ±0.1 G or better. Not only is it questionable whether the field sweep and scan range of the magnet are this accurate, but it is also possible that a slight noncoincidence of the g, A, or Q tensors or a small asymmetry parameter, QE, in the quadrupole tensor, could lead an error of this magnitude in the spacings between the allowed transitions. Intensities of the secondary transitions are especially difficult to measure for copper–sulfur systems, because the small quadrupole coupling constant makes the secondary lines relatively weak.

To analyze the secondary transitions, one must determine all the EPR parameters in the following spin Hamiltonian:

$$\mathcal{H}_s = g_x\beta B_x S_x + g_y\beta B_y S_y + g_z\beta B_z S_z + A_x I_x S_x + A_y I_y S_y + A_z I_z S_z - g_n\beta_n(B_x I_x + B_y I_y + B_z I_z) + QD[I_z^2 - I(I+1)/3] + QE(I_x^2 - I_y^2)$$

All the tensor axes are coincident and the z tensor axis coincides (to a sufficiently good approximation) with the molecular z axis for all the square-planar complexes studied. The nuclear Zeeman interaction must be included because it is of the same order of magnitude as the quadrupole interaction. The nuclear Zeeman interaction also makes a substantial contribution to the forbidden transitions' intensity. In fact, Q-band, 35-GHz, EPR spectra give better quadrupole coupling information than X-band, 9.5-GHz, EPR spectra, because the larger nuclear Zeeman term makes some of the forbidden transitions more intense.

Since the hyperfine interaction is much larger than the nuclear Zeeman and nuclear quadrupole interaction for the copper complexes studied, reasonably accurate g and A values can be obtained from the allowed transitions. The g value can be calculated from the magnetic field position of the center of the outermost hyperfine lines. A values can be calculated from the average spacing between the hyperfine peaks in single-crystal or powder EPR data. The nuclear g value of the ^{63}Cu nucleus is known and assumed to be isotropic. Signs of the hyperfine coupling constants also need to be known; they can be obtained by fitting the experimental line positions of the secondary transitions.

Once g and A values have been determined, theoretical line positions of the forbidden transitions are computed by exact diagonalizations of the 8×8 spin Hamiltonian matrix for the $S = \frac{1}{2}$, $I = \frac{3}{2}$ $^{63}Cu(II)$ systems at all the appropriate orien-

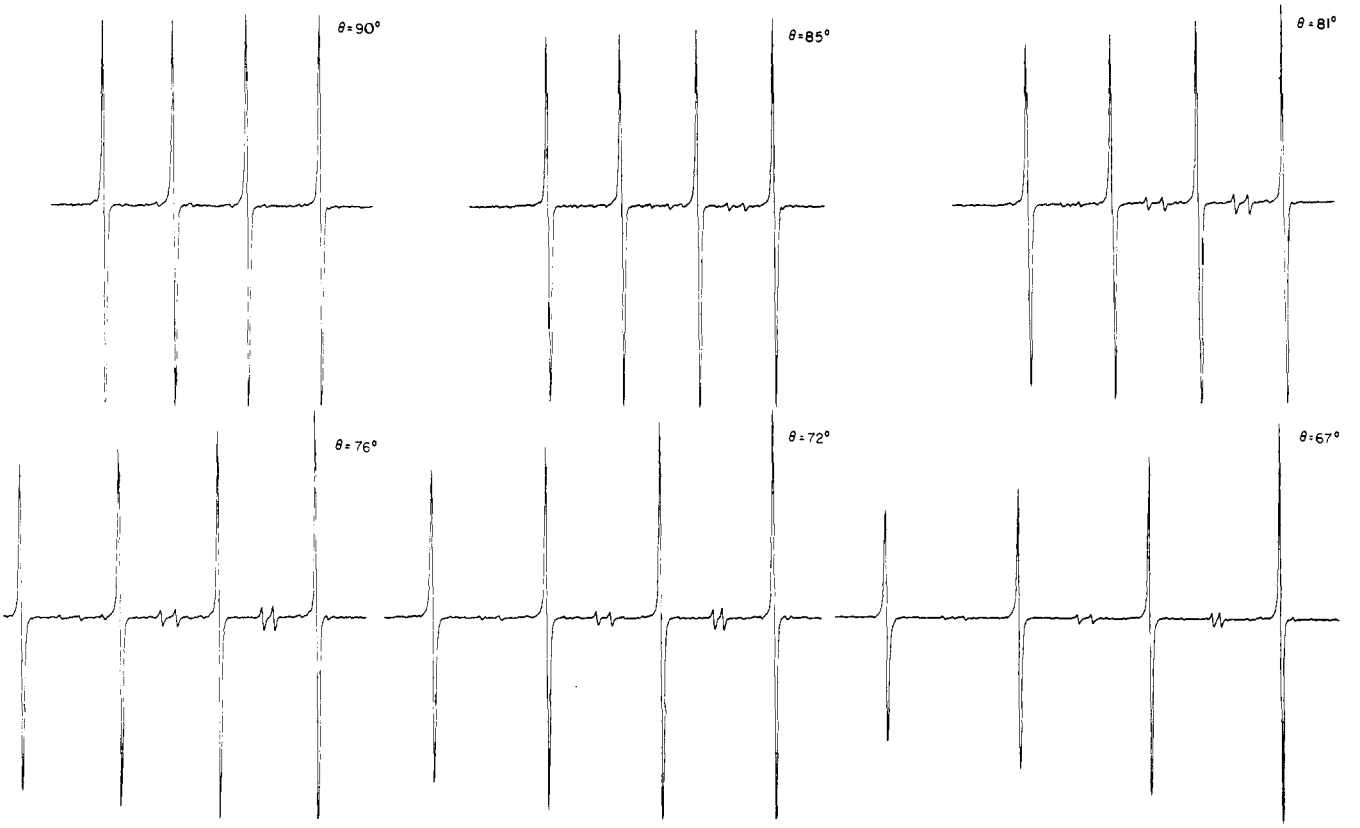

Figure 1. Q-Band (35.0-GHz) first-derivative EPR spectra for a ^{63}Cu-doped single crystal of $[(CH_3)_4N]_2[Ni(mnt)_2]$ at orientations θ = 90, 85, 81, 76, 72, and 67°. The secondary transitions are observed as doublets between the primary transitions.

tations. The theoretical line positions for all the appropriate orientations are compared to the experimental line positions. Relative intensities of the forbidden and allowed transitions can also be computed. The intensity is proportional to the matrix element $\langle n|S_h|m\rangle^2$, where the operator S_h is the spin magnetic dipole component in the direction of the oscillating field, and n and m are the stationary states for the magnetic dipole transition under consideration.

Only the spacings between the secondary doublets need to be examined to obtain quadrupole coupling data. Although they have zero intensity precisely at the θ = 90° orientation, these secondary transitions have appreciable intensity very near the perpendicular (θ = 90°) orientation. For the square-planar copper–sulfur complexes, they are relatively weak but observable. Figure 1 shows the doped single-crystal EPR spectra for a copper–sulfur complex at and near the perpendicular orientation. Note that the $\Delta m_I = \pm 1$ doublets grow in intensity and their spacings vary as the crystal rotates away from the perpendicular orientation. The lines for the square-planar Cu–S complexes in the room-temperature single-crystal EPR spectra are relatively narrow, i.e., approximately 1 G half-width at half-height. The hyperfine structure is highly resolved and the doublet spacings of the secondary transitions are easily measured.

The calculated doublet spacings as they vary with orientation for the low-field (LF), mid-field (MF), and high-field (HF) secondary transitions are shown in Figure 2, along with the experimental data for the $K_2Cu(dto)_2$ complex. The calculated orientation dependence of intensities of the secondary transitions is also included in Figure 2. The HF and LF doublet spacings are sensitive to the magnitude of the quadrupole coupling constant. The MF set, while insensitive to the quadrupole coupling constant, is very sensitive to the magnitude of the nuclear g value. Measuring the HF or LF doublet spacings gives the quadrupole coupling constant, and the MF doublet spacing confirms the magnitude of the copper nuclear

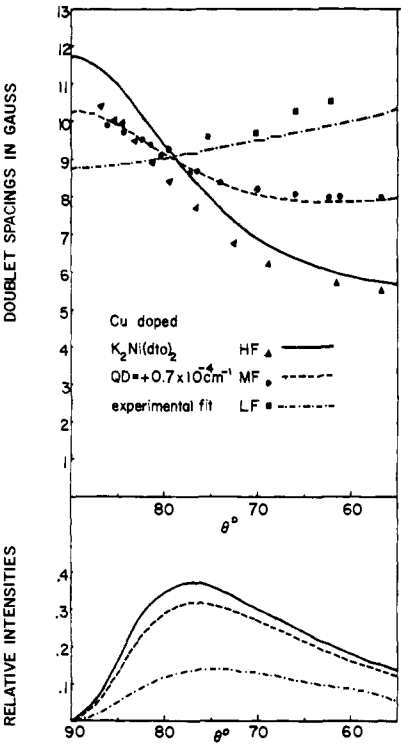

Figure 2. Angular dependence of the LF, MF, and HF secondary ($\Delta m_I = \pm 1$) doublet spacings for $K_2Cu(dto)_2$ over the range of orientations θ = 90 to 55°; relative intensities of the LF, MF, and HF secondary transitions over the same range of orientations at the bottom of the figure. More information on the experimental fit is found in the Appendix. Experimental points are indicated by symbols, calculated values by lines.

g value. The experimental fit for HF and LF spacings for this complex are not as good as would like; the Appendix comments on this point and describes a strategy for extraction of QD.

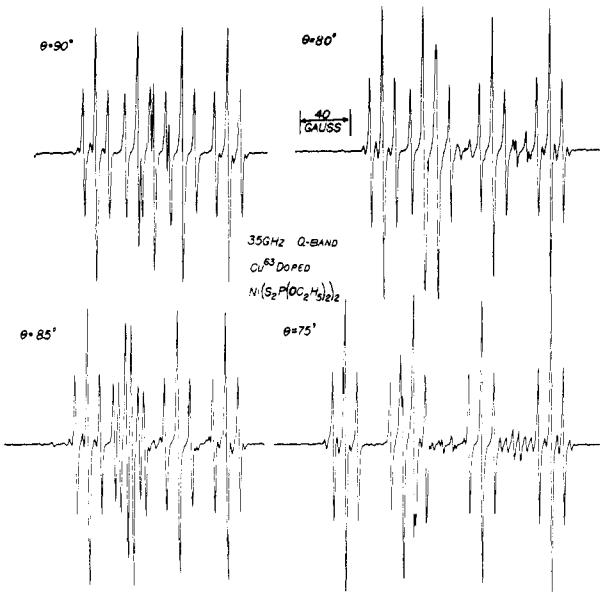

Figure 3. Q-Band (35.0-GHz) first-derivative EPR spectra of a ^{63}Cu-doped single crystal of $Ni(S_2P(OC_2H_5)_2)$ at orientations θ = 90, 85, 80, and 75°. The secondary transitions are observed as two overlapping 1:2:1 triplets between the primary transitions. The overlapping triplet occuring with the second low-field primary triplets is from another magnetic site.

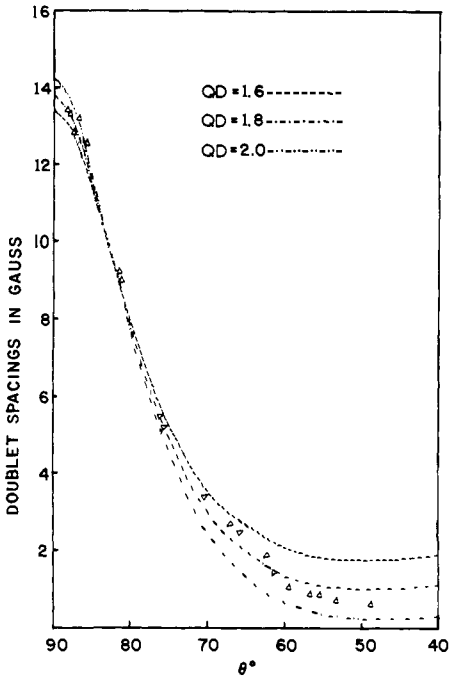

Figure 4. High-field doublet spacings of secondary transitions of Cu-$(S_2P(OEt)_2)_2$ over the range of orientation θ = 90 to 40°. Calculated doublet spacings are included for three quadrupole coupling constants: QD = 1.6, 1.8, and 2.0 × 10^{-4} cm^{-1}. Experimental values are indicated by triangles.

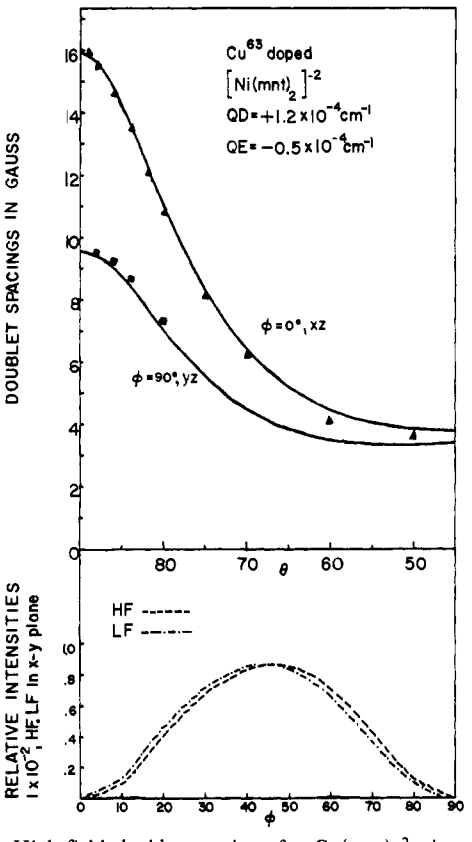

Figure 5. High-field doublet spacings for $Cu(mnt)_2^{2-}$ in xz and yz planes over range of orientations θ= 90 to 45°. QD = 1.2 × 10^{-4} cm^{-1} and QE = −0.5 × 10^{-4} cm^{-1}. The relative intensities of the LF and HF secondary transitions in x-y plane, i.e., ϕ = 0 to 90°, θ = 90°, are shown at bottom of figure.

In previous studies[1-6] of Cu-O complexes, tertiary as well as secondary transitions were visible. The intensity of the tertiary transitions is greatest at θ = 90°, but decreases rapidly away from the perpendicular (θ = 90°) orientation. For the square-planar copper-sulfur complexes the tertiary transitions are not readily observable. Because of their low intensity, they are obscured by the ^{33}S (0.74% natural abundance) ligand superhyperfine structure.

Figure 3 shows the doped single-crystal EPR spectrum of a copper-sulfur complex, $Cu(S_2P(OC_2H_5)_2)$. Here, ligand superhyperfine structure from two equivalent phosphorus atoms, I = ½, is apparent. The secondary lines are observed as 1:2:1 triplets between the primary lines. Quadrupole coupling information was obtained for this complex, but the spectrum's complexity caused by the ligand superhyperfine structure illustrates why it is desirable to study Cu complexes that do not have appreciable superhyperfine structure. The presence of complex superhyperfine structures for Cu complexes having other donor atoms, such as nitrogen and phosphorus, is the primary reason why ^{63}Cu quadrupole coupling data in paramagnetic sites have been obtained mostly for Cu-O and Cu-S complexes.

The calculated HF doublet spacings for three different quadrupole coupling constants and experimental data for the $Cu(S_2P(OC_2H_5)_2)$ complex are shown in Figure 4, which illustrates that the expected accuracy of the quadrupole coupling constant obtained from this EPR technique is ±0.1 × 10^{-4} cm^{-1}.

For two of the complexes studied, an asymmetry parameter, QE, in the quadrupole tensor was needed to interpret their single-crystal EPR spectra even though their g and A parameters were nearly axial. For these complexes the doublet spacings of the HF and LF forbidden transitions are dependent upon φ as well as θ. Also, a nonzero asymmetry parameter causes the HF and LF secondary transitions no longer to have zero intensity at all the θ = 90° orientations; they vanish at θ = 90° only if φ = 0° or 90°. The MF secondary doublets, not very sensitive to the quadrupole term, are unaffected by the addition of the asymmetry term.

Figure 5 shows the variation of the HF secondary doublet spacings with θ orientation for different φ orientations between 0 and 90° for a copper-sulfur complex that has a nonzero QE. It also shows angular dependence of intensities of the HF and

Table I. EPR Parameters for Copper Complexes[a]

Host	g_z	g_x	g_y	A_z	A_x	A_y	QD
$Ni(dto)_2^{2-}$	2.0805	2.0197	2.0191	−163.9	−42.4	−41.6	0.7
$Ni(dtc)_2$	2.0856	2.0227	2.0186	−156.2	−38.5	−34.5	0.7
$Ni(i\text{-}mnt)_2^{2-}$[b]	2.086	2.023	2.019	−156.0	−38.5	−35.0	0.7
$Ni(S_2P(OC_2H_5)_2)_2$	2.0855	2.0199	2.0230	−150.6	−30.5	−32.8	1.8–1.9
$Ni(mnt)_2^{2-}$	2.0837	2.0210	2.0199	−160.5	−39.4	−39.0	1.2
							$QE = -0.5$[c]
$Pd(SdbmO)_2$	2.1450	2.0294	2.0313	−160.5	−35.2	−37.6	1.3
							$QE = 0.4$[c]

[a] All values are for ^{63}Cu. All coupling constants are in 10^{-4} cm^{-1}. EPR parameters were obtained from computer simulations of the EPR powder spectrum and QD from single-crystal EPR spectra. Estimated errors are ±0.0003 for g values, $\pm 0.3 \times 10^{-4}$ cm^{-1} for hyperfine parameters, and $\pm 0.1 \times 10^{-4}$ cm^{-1} for QD and QE. [b] EPR parameters are approximate, similar to those of the $Cu(dtc)_2$ complex. [c] Asymmetry in quadrupole tensor. See Hamiltonian for definition of QE.

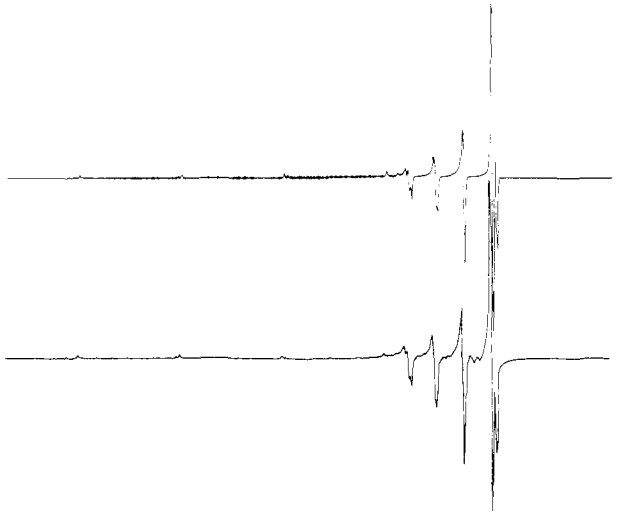

Figure 6. Q-Band first-derivative EPR spectrum of a Cu-doped powder of $K_2Ni(dto)_2$; natural isotopic mixture of ^{63}Cu and ^{65}Cu. The top scan is computer-simulated powder spectrum. The lower scan is the experimental spectrum. The scan range is 11 500–12 500 G, left to right. Both ^{63}Cu and ^{65}Cu species have been included in the simulation for which the ^{63}Cu parameters are $g_x = 2.0197$, $g_y = 2.0191$, $g_z = 2.0806$, $A_x = 0.00424$ cm^{-1}, $A_y = 0.00416$ cm^{-1}, $A_z = 0.01639$ cm^{-1}, $\nu = 34.58$ GHz, Lorentzian line shapes with width = 1.1 G.

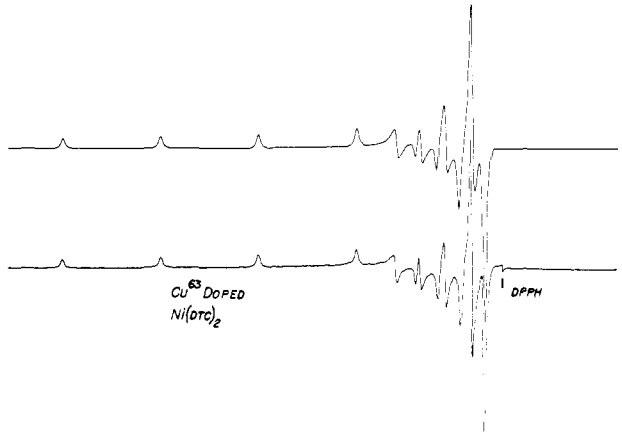

Figure 7. Q-Band first-derivative EPR spectrum of a ^{63}Cu-doped powder of $Ni(dtc)_2$. The top scan is the computer-simulated spectrum. The lower scan is the experimental spectrum. The scan range is 11 500–12 500 G, left to right. The parameters for the simulation are $g_x = 2.0227$, $g_y = 2.0186$, $g_z = 2.0586$, $A_x = 0.00385$ cm^{-1}, $A_y = 0.00345$ cm^{-1}, $A_y = 0.01562$ cm^{-1}, $\nu = 34.54$ GHz, Lorentzian line shapes with width = 4.0 G.

LF secondary doublets within the x-y plane. The experimental data included are for the $Cu(mnt)_2^{-2}$ dianion with **B** in the xz and yz planes. Note the larger variation in the HF doublet spacings with φ near the xy plane and the maximization of intensity of the HF and LF doublets in the xy plane at the $\varphi = 45°$ orientation.

V. Results: Computer Simulations of Powder Spectra and Quadrupole Coupling Parameters

Table I summarizes all the EPR information obtained from computer simulations of powdered samples and the quadrupole coupling parameters obtained from single-crystal studies. The signs on the hyperfine coupling constants were determined from the secondary doublet spacings in the single-crystal EPR spectra. The magnitudes of the g and A values were obtained from computer simulations.

$K_2Cu(dto)_2$. Figure 6 shows a computer simulated and an experimental EPR spectrum of $K_2Ni(dto)_2$ powder doped with natural-abundance Cu. The computer simulation program was modified slightly to include the ^{65}Cu species, 31% natural abundance. Because of its slightly larger nuclear g_n, ^{65}Cu features can be split from ^{63}Cu features. No previous single-crystal EPR studies have been reported, but solution EPR spectra have been observed.[21] The g and A values resemble those found for other square-planar Cu-S complexes. The g anisotropy is slightly smaller and the isotropic part of the hyperfine coupling slightly larger. The presence of small peaks between the larger features in the perpendicular region of the powder spectrum are the secondary "forbidden" resonances. Their intensity is small, as are nuclear Zeeman and quadrupole effects upon the primary transitions.

Although secondary transitions appeared in the Cu-doped single-crystal spectra for both the ^{63}Cu and ^{65}Cu isotopes, quadrupole coupling information was derived only from the ^{63}Cu transitions. The system is nearly axial and single-crystal spectra were obtained for several arbitrary planes of rotation. The quadrupole coupling constant was determined from the HF and LF secondary doublet spacings.

$Cu(dtc)_2$. Figure 7 shows computer simulated and experimental EPR spectra of a ^{63}Cu-doped powder of $Ni(dtc)_2$. They agree quite reasonably. The few small discrepancies may be caused partly or wholly by a slight inaccuracy in the second-order perturbation technique and the exclusion of the nuclear Zeeman and nuclear quadrupole terms. The parallel features are found at the low-field end of the spectrum; the perpendicular, at the high.[32,33]

Previous single-crystal EPR results[32,33] are in reasonable accord with our g and A values. For purposes of analysis this system was assumed to be axial. Single-crystal EPR data were obtained for several arbitrary planes of rotation. The quadrupole coupling parameter agrees well with that reported by So,[5] QD being 0.7×10^{-4} cm^{-1}.

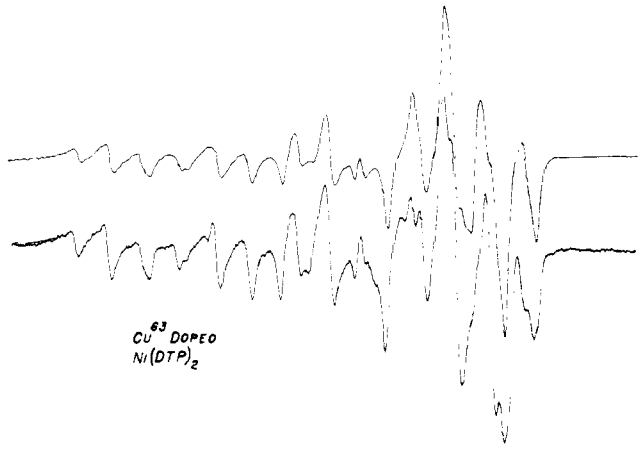

Figure 8. Perpendicular region of the Q-band first-derivative EPR spectrum of a ^{63}Cu-doped powder of $Ni(S_2P(OEt)_2)_2$. The top scan is the computer-simulated spectrum. Lower scan is the experimental spectrum. The scan range, 12 200–12 400 G, left to right, includes only perpendicular features; the parallel region is downfield. Parameters for the simulation are g_x = 2.0199, g_y = 2.0230, g_z = 2.0855, A_x = 0.00305 cm^{-1}, A_y = 0.00328 cm^{-1}, A_z = 0.01506 cm^{-1}, ν = 34.79 GHz, Lorentzian line shapes with width = 1.5 G.

Cu(i-mnt)$_2^{2-}$. The 35-GHz EPR spectrum of a powder of the nickel host, doped with natural-abundance copper, was much like that of the $Cu(dtc)_2$ complex. The EPR parameters are also very similar (see Table I). No previous single-crystal EPR studies have been reported. We assumed this system to be essentially axial and obtained single-crystal EPR data for several arbitrary planes of rotation. The quadrupole coupling constant was 0.7×10^{-4} cm^{-1}.

Cu(S$_2$P(OC$_2$H$_5$)$_2$)$_2$. Figure 8 shows the perpendicular region of computer simulated and experimental EPR spectra of a ^{63}Cu-doped powder of $Ni(S_2P(OC_2H_5)_2)_2$. The parallel resonances are all further downfield, off the graph. The phosphorus superhyperfine structure is apparent and makes the perpendicular features difficult to sort out. Most of the features of the experimental powder spectrum are present in the computer simulation, although the fit is not as good as for our other powder spectra. The small discrepancies in intensity and line positions can easily be due to exclusion of the nuclear Zeeman and nuclear quadrupole terms and possibly to small anisotropies in the phosphorus superhyperfine coupling, which we assumed to be isotropic for purposes of the simulation. The Q-band powder spectrum has resolved an $A_x - A_y$ anisotropy that was not reported in previous single-crystal X-band EPR studies.[34,35] However, the anisotropy is sufficiently slight so that, with little error, we could analyze the single-crystal EPR spectra for quadrupole parameters under an assumption of axial symmetry. Data were collected for several arbitrary planes of rotation and the quadrupole coupling constant was obtained from the HF secondary doublet spacings. The quadrupole term, $\sim 1.8 \times 10^{-4}$ cm^{-1}, is somewhat larger for the $Cu(S_2P(OC_2H_5)_2)_2$ complex than for other copper-sulfur complexes, $\sim 0.7 \times 10^{-4}$ cm^{-1}.

Cu(mnt)$_2^{2-}$. Figure 9 shows the perpendicular region of the computer simulated and experimental EPR spectra of a ^{63}Cu-doped powder of $((CH_3)_4N)_2(Ni(mnt)_2)$. The parallel resonances in the EPR spectrum are further downfield. Forbidden line features are also apparent in the experimental powder spectrum between the allowed-line features in the perpendicular region. Previous single-crystal EPR data are in reasonable agreement with these values.[36]

Our single-crystal EPR studies indicate the quadrupole coupling tensor to have a large asymmetry term, QE. Precession and Weissenberg x-ray photographs of the nickel host crystal were necessary to determine molecular orientations.

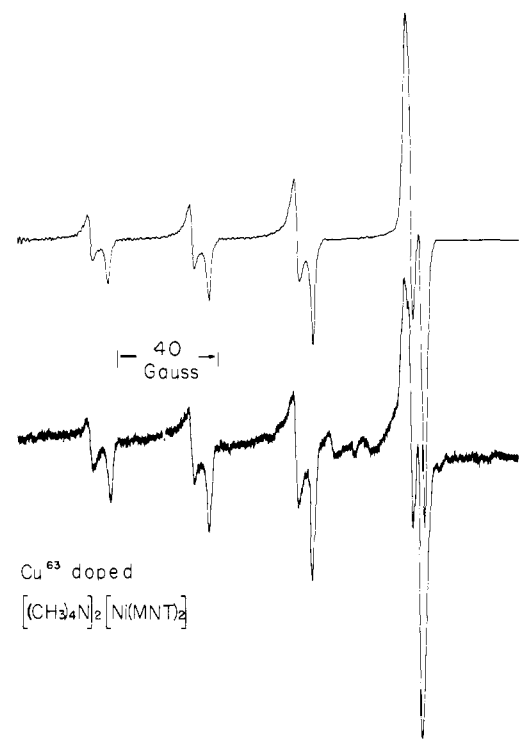

Figure 9. Perpendicular region of the Q-band (35.0-GHz) first-derivative EPR spectrum of a ^{63}Cu-doped powder of $Ni(mnt)_2^{2-}$ dianion. Top scan is the computer-simulated spectrum. Lower scan is the experimental powder spectrum. The scan range, 12 100–12 300 G from left to right, includes only perpendicular features; the parallel region is downfield. Parameters for the simulation are g_x = 2.0210, g_y = 2.0199, g_z = 2.0837, A_x = 0.00394 cm^{-1}, A_y = 0.00390 cm^{-1}, A_z = 0.01605 cm^{-1}, ν = 34.49 GHz, Lorentzian line shapes with width = 1.0 G.

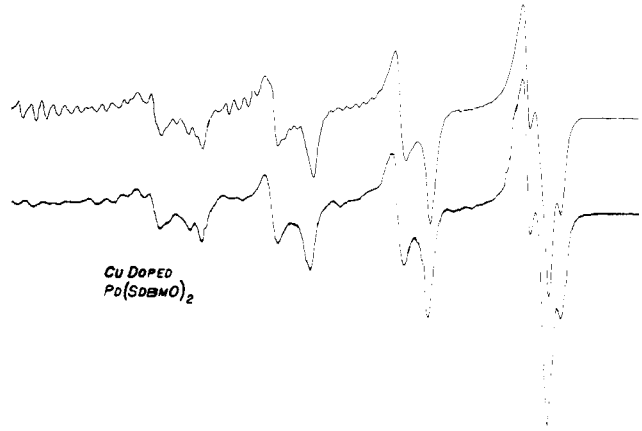

Figure 10. Perpendicular region of the Q-band first-derivative EPR spectrum of a copper-doped powder of $Pd(SdbmO)_2$; natural isotopic mixture of ^{63}Cu and ^{65}Cu. The top scan is the computer-simulated spectrum. The lower scan is the experimental spectrum. The scan range, 12 100–12 300 G, left to right, includes only perpendicular features; the parallel region is downfield. The parameters for the simulation are g_x = 2.2094, g_y = 2.0313, g_z = 2.1450, A_x = 0.00352 cm^{-1}, A_y = 0.00376 cm^{-1}, A_z = 0.01605 cm^{-1}, ν = 34.70 GHz, Lorentzian line shapes with width 1.6 G.

Single-crystal EPR spectra were collected near the x-z and y-z molecular planes and other planes of rotations. The QD value, measured from HF secondary doublet spacings, was 1.2×10^{-4} cm^{-1}; QE was -0.5×10^{-4} cm^{-1} (see Figure 5).

Cu(SdbmO)$_2$. Figure 10 shows the perpendicular region of the computer simulated and experimental EPR spectra for a natural-abundance Cu-doped powder of $Pd(SdbmO)_2$. The computer simulation program was modified to include the ^{65}Cu species. No single-crystal EPR data have been reported for this

Table II. 3d Contribution to the Electric Field Gradient

i, orbital	$\langle 3\cos^2\theta - 1\rangle$	Free ion population (n_i)	$n_i \cdot \langle 3\cos^2\theta - 1\rangle$	$Cu-O_4$ population[a] (n_i)	$n_i \langle 3\cos^2\theta - 1\rangle$	$Cu-S_4$ population[b] (n_i)	$n_i \cdot \langle 3\cos^2\theta - 1\rangle$
$3d_{x^2-y^2}$	−4/7	2	−8/7	1.99	−1.14	1.998	−1.142
$3d_{xy}$	−4/7	1	−4/7	1.37	−0.78	1.560	−0.891
$3d_{yx}$	2/7	2	4/7	1.92	0.55	2.000	0.571
$3d_{xz}$	2/7	2	4/7	1.92	0.55	1.986	0.567
$3d_{z^2}$	4/7	2	8/7	1.98	1.13	1.975	1.129
Sum		9	0.571	9.18	0.310	9.519	0.234
$\langle r^{-3}\rangle \sum_i n_i \langle 3\cos^2\theta - 1\rangle$[c]			4.71 a.u.		2.56 au.		1.93 au.
Covalency reduction factor, f			1.00		0.54		0.41
QD value in 1×10^{-4} cm^{-1}			15.8		8.5		6.5

[a] Mulliken population analysis of molecular orbital coefficients from F. A. Cotton, C. B. Harris, and J. J. Wise, *Inorg. Chem.*, **6**, 909 (1967). [b] Mulliken population analysis of molecular orbital coefficients from C. P. Keijzers, J. M. de Vries, and A. van der Avoird, *Inorg. Chem.*, **11**, 1338 (1972). [c] $\langle r^{-3}\rangle = 8.25$ au.

complex. The principal g values for this mixed sulfur-oxygen donor complex fall between those determined for the square-planar $Cu-O_4$ and $Cu-S_4$ complexes, but are closer to the latter. (The discernible noise in the simulated spectrum is due to graining; i.e., the grid used for calculating the powder spectrum was not fine enough to cancel out all of the off-axis resonances completely.)

Single-crystal EPR studies indicated that the quadrupole coupling tensor had a significant asymmetry term, QE. There are not very good x-ray crystal structure data on record for the Pd host.[31] Precession x-ray photos determined the a, b, and c crystallographic axes. Single-crystal EPR spectra were collected in the ac plane near the x-y molecular plane of one of the magnetic sites and in the bc plane. Directions of the tensor axes were determined from the unit cell illustration depicting the a, b, and c axes in relation to the molecular orientation, as found in the literature.[31] The parameters so determined are $QD = 1.3 \times 10^{-4}$ cm^{-1} and $QE = 0.4 \times 10^{-4}$ cm^{-1}.

VI. Discussion

The quadrupole coupling data in Table I reveal several points of interest, including the following:

(1) The most striking feature is that all of the square-planar Cu(II)-sulfur complexes display considerably smaller coupling constants ($0.6 \leq QD \leq 1.9 \times 10^{-4}$ cm^{-1}) than observed for any of the previously studied square-planar Cu(II)-oxygen or any other $Cu-O_n$ complexes (compare $Cu(acac)_2$ $QD = 3.5 \times 10^{-4}$ cm^{-1}, $Cu(C_2O_4)_2^{-2}$ $QD = 4.5 \times 10^{-4}$ cm^{-1}, up to ~10-11 $\times 10^{-4}$ cm^{-1} for near-octahedral CuO_6 systems).

(2) $Cu(S_2P(OC_2H_5)_2)_2$ exhibits a larger quadrupole coupling constant ($QD = 1.8 \times 10^{-4}$ cm^{-1}) than do other sulfur complexes (~0.7×10^{-4} cm^{-1}).

(3) The $Cu(mnt)_2^{2-}$ anion and $Cu(SdbmO)_2$ chelate display large asymmetry parameters, QE.

The following discussion addresses each of these points in turn.

Point 1. Calculating the electric field gradient (EFG) at the quadrupole nucleus, essential to the interpretation of quadrupole coupling data, involves approximating the electron and nuclear charge distributions of the ligands and the electron populations of the valence orbitals of the quadrupolar nucleus. The valence and ligand electrons can perturb the electrons in the inner shells around the quadrupolar nucleus to give a different effective EFG.[37] Thus, in a drastic approximation which is intuitively useful and makes for tractability, we have divided the EFG into two contributions, one from the valence electrons and the other from the ligand electrons and nuclei:

$$eq = (1 - \gamma_\infty)eq_{\text{lig}} + (1 - R_{3d})eq_{\text{val}}$$

The quantity $(1 - R_{3d})$ is the Sternheimer shielding factor[10] for the valence 3d electrons of the Cu(II) ion; $(1 - \gamma_\infty)$ is the Sternheimer antishielding factor for the ligand electrons. Both are corrections for an original neglect of quadrupolar interactions in the electronic structure calculations. These shielding factors, $(1 - R_{3d})$ and $(1 - \gamma_\infty)$, can be vastly different from each other since they describe the ability of EFG of close-in valence and far-away ligand electrons, respectively,[37] to quadrupolarize the core.

If one could prepare a bare Cu^{2+} ion with the unpaired electron in the d_{xy} orbital, the ground state for the square-planar Cu(II) complex, one would calculate an EFG corresponding to a $QD = 15.8 \times 10^{-4}$ cm^{-1} (see Table II):[5]

$$eq_{\text{val}} = \langle 1/r^3\rangle \langle 3(\cos\theta)^2 - 1\rangle eq_{\text{atomic}}$$

The QD value observed for square-planar Cu(II) complexes, considerably smaller than 15.8, reflects both the change in the electron distribution of the valence orbitals when ligand electrons have bonded to metal orbitals and the contribution to the EFG of the ligands themselves.

To analyze the electron distribution in the valence metal orbitals in square-planar complexes, we have examined a self-consistent field, extended-Hückel molecular orbital calculation for a model CuO_4 complex, copper formylformate $Cu(ff)_2$,[38] and a CuS_4 complex, $Cu(dtc)_2$.[39,40] The Mulliken populations[41] of the copper 3d orbitals generated the contribution of the valence orbitals to the EFG (see Table II). ($Cu(ff)_2$ would be much like $Cu(acac)_2$, and calculations for the former will be applied to the latter.)

For the CuO_4 complex, the valence orbital contribution to QD is reduced to 8.5×10^{-4} cm^{-1}. That is, the free ion EFG is reduced by a factor of 0.54, the covalency reduction factor f: $eq_{\text{valence}} = feq_{\text{atomic}}$. For the model CuS_4 complex, the valence orbital contribution to QD is even further reduced to 6.5×10^{-4} cm^{-1}, with a covalency factor of 0.41. The reduced valence orbital contribution is primarily due to the more populated d_{xy} ground state orbital. There is more donation of ligand electrons to the metal d_{xy} orbital in the CuS_4 complex than in the Cu-O complex because of the larger σ-covalency of the Cu-S bond.

Both calculated quadrupole coupling constants are still much larger than the measured QD values of 3.5×10^{-4} cm^{-1} for $Cu(acac)_2$ and other copper β-keto enolates and 0.7×10^{-4} cm^{-1} for $Cu(dtc)_2$, but the contribution from the ligand electrons and nuclei has not yet been considered. Reduction of the calculated QD to 3.5×10^{-4} cm^{-1}, requires a -5.0×10^{-4}

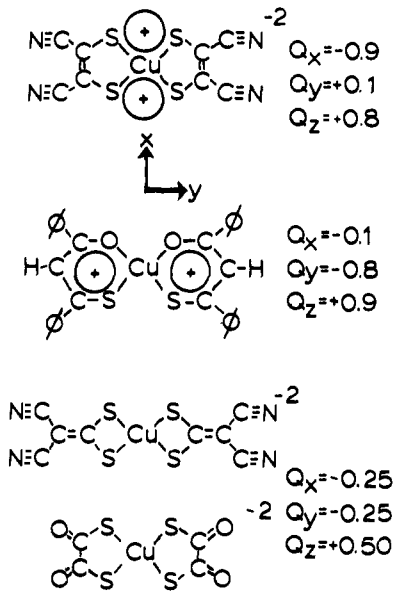

Figure 11. Structures and quadrupole tensor data for four square-planar complexes. From top to bottom: $Cu(mnt)_2^{2-}$, $Cu(SdbmO)_2$, $Cu(i\text{-}mnt)_2^{2-}$, and $Cu(dto)_2^{2-}$. The quadrupole tensor is essentially the same for the latter two complexes. The observed sign of *QD* could, in each case, be produced by regions of electron surplus near the *z* axis (out of the molecular plane); in addition, the large *QE* values for the first two systems could be produced by regions of electron deficiency as indicated by the circled + signs.

ligand contribution for $Cu(acac)_2$. For $Cu(dtc)_2$ a very similar ligand contribution, -5.8×10^{-4} cm^{-1}, will produce the desired 0.7×10^{-4} cm^{-1}.

To calculate ligand contributions of this magnitude,[42,43] we have had to apply Sternheimer antishielding constants in the reasonable range $1 - \gamma_\infty = 10\text{-}15$.[5,42] In summary, we propose that most of the reduction in the quadrupole coupling constant for the Cu-S complexes is caused simply by the increased covalency of the Cu-S σ bond, and that it is a direct reflection of increased occupancy of the dδ orbitals of copper.

Point 2. The quadrupole coupling constant for the $Cu(S_2P(OEt)_2)_2$ complex is 1.8×10^{-4} cm^{-1}, while those of other Cu-S complexes were $\sim 0.7 \times 10^{-4}$ cm^{-1}. This enhancement is intriguing; however, we emphasize that all the quadrupole coupling differences among the CuS_4 and CuS_2O_2 systems are subtle effects which can be caused by redistribution of 0.1 e$^-$ within the Cu valence shell. We have attributed enhancement of Cu quadrupole coupling to either decreased π back-bonding ($Cu(C_2O_4)_2^{2-}$ vs. $Cu(acac)_2$)[6] or, as discussed in Point 1, decreased σ bonding. One might expect the sp^3 hybridization of the phosphorus atom to reduce π bonding of the metal-ligand ring system. Although the Mulliken populations[39,40] of d_{xz} and d_{yz} for $Cu(dtc)_2$ indicate little delocalization of the electrons in these orbitals, we must interpret them with caution because of the limitations inherent in the molecular orbital treatment, which did not include d orbitals on sulfur atoms. The other possibility is that the Cu-S bond is less covalent than for other copper-sulfur complexes, putting less electron density into the d_{xy} orbital on the metal. However, the Cu-S bond lengths and the covalency of the Cu-S bond are nearly the same as those for other copper-sulfur complexes.[44]

To increase the valence orbital contribution to the electric field gradient by 1.0×10^{-4} cm^{-1} *QD* units to account for the larger quadrupole coupling constant, one need remove only $\sim$0.07 e from a d_{xy} or $d_{x^2-y^2}$ orbial. Phosphorus superhyperfine coupling constant data from the EPR spectra may provide a clue.[45-49] The phosphorus superhyperfine coupling constant in $Cu(S_2P(OEt)_2)_2$ is approximately 10 G and nearly isotropic. Appreciable spin density is being delocalized onto the phosphorus 3s orbital. Wasson[49] suggest that this delocalization must take place via the sulfur atoms. To fit in with the quadrupole coupling data and maintain the large covalency of the Cu-S bond, the spin delocalization must be greater than that of the other Cu-S complexes and must not occur through the Cu-S bonding mechanism. The other possibility is that electron density has been removed from the occupied $d_{x^2-y^2}$ orbital. The large phosphorus superhyperfine coupling for the $VO(S_2P(OEt)_2)_2$ complex, $\sim$40 G, suggests that a direct overlap of the phosphorus 3s orbital with the ground state $d_{x^2-y^2}$ orbital is the primary mechanism for the spin delocalization. A similar transannular overlap may be present in the $Cu(S_2P(OEt)_2)_2$ complex. However, one might expect to find an asymmetry parameter associated with this type of delocalization; no large *QE* was found for the Cu complex. Still, the latter possibility seems the most plausible. The coefficient of the phosphorus 3s orbital (c_s) in the molecular orbital containing the unpaired electron can be calculated from the magnitude of the phosphorus superhyperfine coupling constant.[50]

$$^{31}P A = (8\pi/3) g_e g_e \beta_e \beta_n |\psi\ 3s(0)|^2 c_s^2$$

The values of c_s^2 for the VO^{2+} and Cu^{2+} complexes are 0.0135 and 0.0026, respectively.[49] Assuming the coefficient for the $d_{x^2-y^2}$ overlap interaction is the same magnitude in the $Cu(S_2P(OEt)_2)_2$ as in the VO^{2+} complex, we find that the $|c_s|$, $\sim$0.1161, can easily account for a 0.07 reduction in the Mulliken population of the $d_{x^2-y^2}$ orbital. The question is whether the same sort of interaction is present in the other CuS_n complexes, particularly the $Cu(dtc)_2$ complex, with a similar four-membered ring structure. No data have been collected on the ^{13}C superhyperfine coupling for the VO^{2+} or Cu^{2+} complexes, but one might expect less overlap with the valence 2s orbital on carbon than with the valence 3s orbital on phosphorus. The expected concomitant asymmetry parameter may be attenuated by other types of electronic interactions in the $Cu(S_2P(OEt)_2)_2$ complex.

In order to explore these points, we have in progress quadrupole coupling studies on other Cu(II) compounds having both S and P atoms.

Point 3. Although most square-planar copper-sulfur complexes have only a small asymmetry parameter, we found *QE* to be very large in $Cu(mnt)_2^{2-}$. Figure 11 compares important structural features and the quadrupole coupling tensor parameters for $Cu(mnt)_2^{2-}$ and other copper-sulfur complexes. The main structural feature unique to the $Cu(mnt)_2^{2-}$ complex is the presence of the double bond in the ligand. The C-C bond length is 1.32 Å, while that for the structurally similar $Cu(dto)_2^{2-}$ complex is 1.52 Å. The EPR parameters for $Cu(mnt)_2^{2-}$ are much like those of other Cu-S complexes (see Table I), but other physical properties differ dramatically. For example, in the visible spectrum the first d-d transition is observed at much lower energy,[51] the oxidation potential is significantly lower,[52] and a stable $Cu(mnt)_2^-$ monoanion has been isolated.[53]

In an attempt to discover whether the double bond on the ligand is the significant feature that contributes to the asymmetry in its quadrupole coupling tensor, we did a rough point-charge calculation. Placing a point-charge equivalent to that of 0.5 e at the center of the double bond in each ligand is enough to account for the observed asymmetry in the quadrupole coupling. The charge distribution provided by a molecular orbital calculation for ethylene[54] suggests that this explanation is reasonable. Placing two ethylene groups at the approximate positions of the mnt ligand in the $Cu(mnt)_2^{2-}$ complex and considering the Mulliken populations of the valence orbital on the carbon atoms, we indeed find contributions sufficiently large to account for the asymmetry parameter. On the other hand, the mnt ligand double bond could be different

from that in ethylene; nitrile groups (-C≡N) are σ and π acceptors and so are the mercapto groups (-SH). Thus, this calculation does not rule out the possibility that the asymmetry parameters arise from the valence contribution to the EFG. The large splitting in energy of the d_{yz} and d_{xz} orbitals postulated for this complex would be consistent with an imbalance between the d_{yz} and d_{xz} populations.[55] A possible mechanism for this sort of electron distribution would be the formation of a π bond between the d_{yz} orbital and the double bond on the ligand. (But this "bond" would be 3.0 Å long!)

Solution EPR and visible spectra of $Cu(mnt)_2^{2-}$ in strong nucleophiles, e.g., pyridine, show no axial interactions with the solvent. This suggests that the orbitals which would be involved in axial coordination are already involved in the bonding elsewhere in the complex. Evidently, this particular complex has a strong and complex π-bonding scheme. In order to generate the large quadrupole asymmetry, it must distribute electrons so as to concentrate them near the y molecular axis and away from the x molecular axis. It must also account for the slight increase in the QD value to 1.2 from 0.7 for square-planar copper complexes.

The other complex exhibiting substantial asymmetry is $Cu(SdbmO)_2$. This mixed S-O donor atom complex has a quadrupole coupling parameter resembling that of a $Cu-S_4$ square-planar complex. Apparently, the strongly covalent Cu-S bonds dominate. The magnitude of the asymmetry parameter is similar to that observed for the $Cu(mnt)_2^{2-}$ complex, but the sign of QE is different. The axis with a deficiency of electrons in the x-y plane is now along the y axis rather than the x axis. It is pointless to speculate on the origin of the asymmetry parameter in this complex, since there are only incomplete structural data for the complex and it is as yet a single isolated curiosity. It may be that the copper β-keto enolates, the $Cu-O_4$ analogues of $Cu(SdbmO)_2$, also have slight asymmetry parameters. (A small asymmetry has been reported[56] for square-planar $Mn(acac)_2$ complex.) Asymmetry was not the focus of our previous studies[5] on CuO_n systems, and some could have gone undetected.

Summary

The quadrupole coupling constants of square planar Cu-S complexes are positive but quite small, characteristic of a *nearly* spherical charge distribution about the Cu nucleus. Two opposing contributions can account for the small magnitude of the quadrupole coupling constant, a negative contribution from the ligand in the xy plane and a slightly larger positive contribution from the electron hole in the d_{xy} valence orbitals. Although variations observed in the quadrupole coupling appear to be related mainly to changes in the distribution of electrons in the 3d valence orbitals, there are anomalies which imply that the coupling tensor is sensitive to the covalency of the metal-ligand bond, the metal-ligand π-bonding in the complex, and possibly to bonding effects of atoms that are not directly bonded to the metal ion. Clearly, the quadrupole coupling parameters provide significant information which can help to elucidate the electronic structure of transition metal complexes. Here, supplementing our previous demonstrations of a strong and interpretable correlation of e^2qQ with electronic and molecular structures in CuO_n systems, we have established correlation of e^2qQ with the bonded atom through study of several CuS_4 and CuS_2O_2 systems.

Added Note. Since submission of this paper, there has been a recent report[57,58] of quadrupole coupling parameters for $Cu(dtc)_2$ in the $Zn(dtc)_2$ host lattice, which has a dimeric structure creating a distorted tetragonal (CuS_5) pyramid of coordination. The reported $QD = 3.15 \times 10^{-4}$ cm^{-1} (with $QE = 0.55 \times 10^{-4}$ cm^{-1}) is quite in line with the trends reported here. The axial ligand should contribute a positive increment to QD, just as we have experimentally[5] and computationally[42] found a fifth, axial O atom to do in CuO_n compounds. In fact, the crudest sort of modification of our simple computations, attributing the semiempirical -5.8×10^{-4} cm^{-1} contribution to two axial holes in a coordination octahedron and thus reducing it by half when one of the holes is filled by the fifth ligand, would yield a surprisingly good *predicted* QD of 3.6×10^{-4} cm^{-1}.

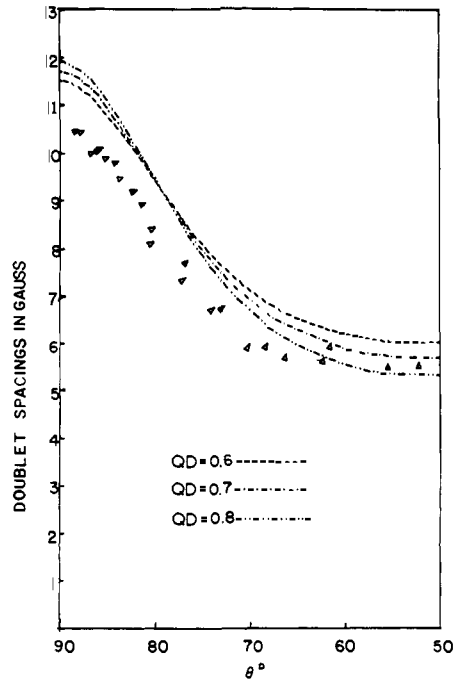

Figure 12. Angular dependence HF secondary doublet spacings of $K_2Cu(dto)_2$, θ = 90 to 50°. The calculated doublet spacings are included for three quadrupole coupling constants: QD = 0.6, 0.7, and 0.8 × 10^{-4} cm^{-1}. Experimental points are indicated by triangles. See Appendix for interpretation.

Acknowledgment. For helpful discussions and information we thank Drs. E. K. Barefield, G. M. Woltermann, and J. R. Pilbrow. We are grateful for research support provided by the donors of the Petroleum Research Fund, administered by the American Chemical Society, and by the National Science Foundation.

Appendix: Experimental Fits for $\Delta m_I = \pm 1$ Forbidden Lines

The fit between calculated and experimental secondary line pair spacings for the $K_2Cu(dto)_2$ complex shown in Figure 2 is not as good as one would like. Only the MF doublet spacings, which are not very sensitive to quadrupole parameters, agree well with the calculated spacings. However, the MF secondary doublets do indicate that the sign and magnitude of the nuclear Zeeman term is correct and that the nuclear Zeeman tensor is essentially isotropic. Different signs for quadrupole coupling and hyperfine coupling constants were tried with disastrous results. The difficulty in fitting the HF doublet spacings vs. θ, for our negative hyperfine coupling constants and positive quadrupole coupling constants, is shown in Figure 12. Note that the calculations could reproduce either the shape or the magnitude at given θ, but not both simultaneously to better than ~1 G. So[4,5] encountered a similar problem in attempting to fit the $Cu(dtc)_2$ HF and LF secondary doublets. Slight noncoincidences of the principal axes of A, g, or Q tensors, or a small but nonzero asymmetry parameter, QE, may account for the discrepancies in the HF and LF doublet spacings. Proper definition of these effects would require more detailed data than we have accumulated. However, since we are mainly

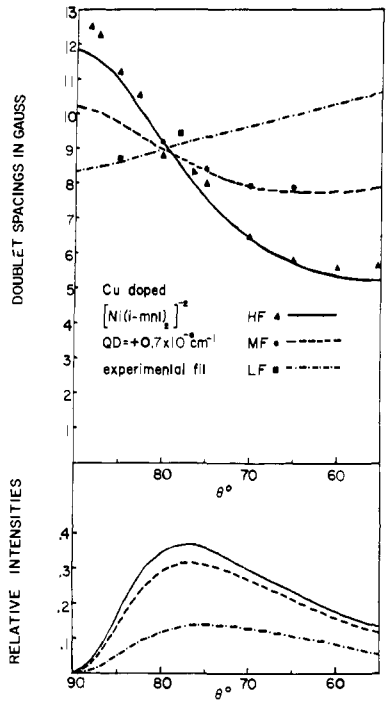

Figure 13. LF(■), MF (●), and HF (▲) secondary ($\Delta m_I = \pm 1$) doublet spacings for $Cu(i\text{-}mnt)_2^{2-}$ over the range of orientations θ = 90 to 55°. Curves calculated for $QD = 0.7 \times 10^{-4}$ cm^{-1} are included (HF—, MF- - -, LF ----). The relative intensities of the LF, MF, and HF secondary transitions over the same range of orientations are at the bottom of the figure. Weakness of the secondary lines made their spacings difficult to measure accurately for $\theta > 85°$; accordingly, no significance should be attached to the minor discrepancies between experimental and HF spacings for large θ.

interested in the values of QD, we have employed an alternative strategy, namely, to fit HF and LF doublet spacings at orientations least sensitive to orientation error and the asymmetry parameter, QE. Orientations from θ = 65 to 50° are the most sensitive to QD and least sensitive to orientation error and the asymmetry parameter. Thus, for $K_2Cu(dto)_2$ and $Cu(dtc)_2$, the QD values that generated the best fits to the HF doublet spacings at these orientations were adopted.

Figure 13 shows the calculated vs. experimental secondary doublet spacings as functions of θ for $Cu(i\text{-}mnt)_2^{2-}$ dianion. Over the entire angular range, the fit is reasonable (i.e., the discrepancy is commensurate with experimental error) for the HF and LF doublet spacings; we needed to select no special orientation to extract the QD of 0.7×10^{-4} cm^{-1}.

References and Notes

(1) B. Bleaney, *Philos. Mag.*, **42**, 441 (1951).
(2) B. Bleaney, K. D. Bowers, and M. H. L. Pryce, *Proc. R. Soc. London, Ser. A*, **228**, 166 (1955).
(3) B. Bleaney, K. D. Bowers, and D. J. E. Ingram, *Proc. R. Soc. London Ser. A*, **228**, 147 (1955).
(4) H. So and R. L. Belford, *J. Am. Chem. Soc.*, **91**, 2392 (1969).
(5) H. So, Ph.D. Thesis, University of Illinois, Urbana, Ill., 1970.
(6) L. K. White and R. L. Belford, *Chem. Phys. Lett.*, **37**, 553 (1976).
(7) H. B. G. Casimir, *Arch. Mus. Teyler, Sect. III*, **8**, 201 (1936).
(8) T. P. Das and E. L. Hahn, "Nuclear Quadrupole Resonance Spectroscopy", Academic Press, New York, N.Y., 1958.
(9) E. A. C. Lucken, "Nuclear Quadrupole Coupling Constants", Academic Press, New York, N.Y., 1969.
(10) G. H. Fuller and V. W. Cohen, *Nucl. Data, Sect. A*, **5**, 446 (1969).
(11) R. M. Sternheimer, *Phys. Rev.*, **164**, 10 (1967).
(12) A. D. Toy, S. H. H. Chaston, J. R. Pilbrow, and T. D. Smith, *Inorg. Chem.*, **10**, 2219 (1971).
(13) J. R. Pilbrow, private communication.
(14) J. R. Pilbrow and M. E. Winfield, *Mol. Phys*, **25**, 1073 (1973).
(15) R. M. Golding, "Applied Wave Mechanics", Van Nostrand, London, 1969, pp 452–454.
(16) J. R. Pilbrow, *Mol. Phys.*, **16**, 307 (1969)
(17) V. I. Krylov, "Approximate Calculation of Integrals", Macmillan, New York, N.Y., 1962, pp. 172, 337.
(18) H. O. Jones and H. S. Tasker, *J. Chem. Soc*, 1904 (1909).
(19) E. G. Cox, W. Wardlaw, and K. C. Webster, *J. Chem. Soc.*, 1475 (1935).
(20) M. Bonamico, G. Dessy, C. Mariani, A. Vaclazo, and L. Zambonelli, *Acta Crystallogr.*, **19**, 619 (1965).
(21) R. Gomper and E. Kutler, *Angew. Chem.*, **74**, 251 (1962).
(22) B. G. Werden, E. Billig, and H. B. Gray, *Inorg. Chem.*, **5**, 78 (1966).
(23) Q. Fernando and C. D. Green, *J. Inorg. Nucl. Chem.*, **29**, 647 (1967).
(24) J. F. McConnell and V. Kastalsky, *Acta Crystallogr.*, **22**, 853 (1967).
(25) G. Bahr and G. Schleitzer, *Chem. Ber.*, **88**, 1771 (1955); **90**, 438 (1957).
(26) E. Billig, R. Williams, I. Bernal, J. H. Waters, and H. B. Gray, *Inorg. Chem.*, **3**, 663 (1964).
(27) R. Eisenberg, J. A. Ibers, R. J. H. Clark, and H. B. Gray, *J. Am. Chem. Soc.*, **86**, 113 (1964).
(28) R. Eisenberg and J. A. Ibers, *Inorg. Chem.*, **4**, 605 (1965).
(29) S. H. H. Chaston, S. E. Livingstone, J. N. Lockyer, V. A. Pickles, and J. S. Shannon, *Aust. J. Chem.*, **18**, 673 (1965).
(30) S. H. H. Chaston and S. E. Livingston, *Aust. J. Chem.*, **20**, 1065 (1967).
(31) E. A. Shugam, L. M. shkol'nikova, and S. E. Livingstone, *J. Struct. Chem. (Engl. Transl.)*, **8**, 490 (1967).
(32) T. R. Reddy and R. Srinivasan, *J. Chem. Phys.*, **43**, 1404 (1965).
(33) M. J. Weeks and J. P. Fackler, *Inorg. Chem.*, **7**, 2548 (1968).
(34) R. K. Cowsik and R. Srinivasan, *Chem. Phys. Lett.*, **16**, 183 (1972).
(35) R. K. Cowsik and R. Srinivasan, *J. Chem. Phys.*, **59**, 5517 (1973).
(36) A. H. Maki, N. Edelstein, A. Parison, and R. H. Holm, *J. Am. Chem. Soc.*, **86**, 4580 (1964).
(37) R. M. Sternheimer, *Phys. Rev.*, **95**, 736 (1954); **105**, 158 (1957).
(38) F. A. Cotton and J. J. Wise, *Inorg. Chem.*, **6**, 909 (1967); **5**, 1200 (1966).
(39) C. J. Keijzers, H. J. M. deVries, and A. Van der Avoird, *Inorg. Chem.*, **11**, 1338 (1972).
(40) C. J. Keijzers, private communications.
(41) R. S. Mulliken, *J. Chem. Phys.*, **23**, 1833 (1955).
(42) H. So, D. Huang, L. K. White, and R. L. Belford, submitted for publication; L. K. White, Ph.D. Thesis, University of Illinois, 1975; D. T. Huang, Ph.D. Thesis, University of Illinois, 1971.
(43) For $Cu(ff)_2$, the calculated ligand contribution is quite reasonable For $Cu(dtc)_2$, a bit more electron density has to be on the sulfur atoms. Possibly the required extra electron population would be accommodated by mixing in of sulfur d orbitals, which were excluded from the MO model.
(44) R. Eisenberg, *Prog. Inorg. Chem.*, **12**, 295 (1970).
(45) N. S. Garif'yanov and B. M. Kozynev, *J. Struct. Chem. (Engl. Transl.)*, **6**, 734 (1965).
(46) N. S. Garif'yanov, B. M. Kozynev, and I. F. Gainullin, *J. Struct. Chem. (Engl. Transl.)*, **9**, 451 (1968).
(47) R. G. Cavell, E. D. Day, W. Byers, and P. M. Watkins, *Inorg. Chem.*, **11**, 1591 (1972).
(48) J. P. Wasson, G. M. Woltermann, and H. S. Stoklosa, *Fortschr. Chem. Forsch.*, **35**, 65 (1973).
(49) J. R. Wasson, *Inorg. Chem.*, **10**, 1531 (1971).
(50) A. Carrington and A. D. McLachlan, "Introduction to Magnetic Resonance", Harper and Row, New York, N.Y., 1967, p 80.
(51) H. B. Gray, *Trans. Metal. Chem.*, **1**, 240 (1965).
(52) A. Davison, N. Edelstein, R. H. Holm, and A. H. Maki, *J. Am. Chem. Soc.*, **85**, 2029 (1963).
(53) A. Davison, N. Edelstein, R. H. Holm, and A. H. Maki, *Inorg. Chem.*, **2**, 1227 (1963).
(54) L. C. Snyder and H. Basch, "Molecular Wave Functions and Properties", Wiley, New York, N.Y., 1972, T56.
(55) S. I. Shupack, E. Billig, R. J. H. Clark, R. Williams, and H. B. Gray, *J. Am. Chem. Soc.*, **86**, 4594 (1964).
(56) C. J. O'Conner and R. L. Carlin, *Inorg. Chem.*, **14**, 291 (1975).
(57) C. P. Keijzers. P. L. A. C. M. van der Meer, and E. de Boer, *Mol. Phys.*, **6**, 1733 (1975).
(58) C. P. Keijzers and E. de Boer, *Mol. Phys.*, **6**, 1743 (1975).